Multiple Convection Patterns and Thermohaline Flow in an Idealized OGCM

STEFAN RAHMSTORF

Institut für Meereskunde, Universität Kiel, Kiel, Germany

(Manuscript received 17 June 1994, in final form 7 April 1995)

ABSTRACT

This paper investigates how multiple steady states arise in an ocean general circulation model, caused by the fact that many different convection patterns can be stable under the same surface boundary conditions. Two alternative boundary conditions are used in the experiments: classical mixed boundary conditions and a diffusive atmospheric heat balance combined with fixed salt fluxes.

In both cases, transitions between different quasi-steady convection patterns can be triggered by briefly adding fresh water at convection sites. Either a large-scale freshwater anomaly is used to completely erase the previous convection pattern or a "surgical" anomaly is added to single grid points to turn off convection there.

Under classical mixed-boundary conditions, different convection sites can lead to different overturning rates of deep water. The dynamics of the convection-driven flow is analyzed in some detail.

With an energy balance atmosphere, in contrast, the overturning rate is very robust, apparently regulated by a negative thermal feedback. In spite of this, different convection patterns are associated with very different climatic states, since the heat transport of the deep circulation depends strongly on where convection takes place. It is suggested that considerable climate variability in the North Atlantic could be caused by changes in high-latitude convection.

1. Introduction

a. Convection and thermohaline flow

Deep convection is a crucial link in the global overturning motion of the oceans, known as the Great Ocean Conveyor Belt. The water masses that fill the deep ocean basins all originate in a few relatively small convection regions in high latitudes. There are two distinct processes acting jointly to form these deep water masses. The first is convection, which for the large-scale flow is essentially a mixing process, homogenizing water properties in the vertical (Send and Marshall 1995). The second process is downward advection or sinking, which is obviously required for continuity reasons if deep water is to spread away from the formation regions at depth. In hydrostatic models the two processes are strictly separate; convection is parameterized as complete (or at least very vigorous) vertical mixing, or sometimes as "layer swapping," while vertical velocities are computed from the divergence of horizontal flow.

There are some general comments that can be made about the role of convection for the large-scale, long-term mean flow. Sandström's theorem [Sandström (1908); see Colin de Verdière (1993) for a recent discussion] states that diabatic volume expansion (i.e., heating, if we consider just thermal forcing for the moment) will lead to an overturning circulation if, and only if, it occurs at greater depth than the corresponding cooling. Differential surface heating cannot directly cause deep flow; it is the downward penetration of heat by diffusion that provides the deep heat source driving the circulation. The balancing upward heat flow occurs in regions with inverse temperature gradient, that is, statically unstable regions with vertical convection or flow down a slope. Since this upward heat transport is much more vigorous than downward diffusion through stably stratified waters, only very small convection regions are required to balance the global downward heat flux. In the long-term mean, the deep circulation is thus "pulled" by downward diffusion of heat, which gradually erodes stratification until in some places the water column becomes unstable and convection starts. This convection and the associated deep flow of dense water can then establish a steady balance with downward diffusion, or, in some model studies (e.g., Winton and Sarachik 1993), it can occur in brief violent flushes followed by long periods of stable stratification.

Since the circulation is ultimately "pulled" by diffusion, we should be able to estimate the expected magnitude of thermohaline transports in the oceans from the vertical mixing intensity and the equator to pole temperature range ΔT. We can use the thermal wind equation to obtain a velocity scale depending on the thermal structure:

Corresponding author address: Dr. Stefan Rahmstorf, Institut für Meereskunde, Universität Kiel, Düsternbrooker Weg 20, D-24105 Kiel, Germany.
e-mail: srahmstorf@ifm.uni-Kiel.d400.de

$$u = \frac{g\alpha}{2\Omega}\frac{D}{L}\Delta T, \quad (1)$$

where Ω is the angular frequency of the earth, α is the thermal expansion coefficient, L is a horizontal length scale, and D is the scale depth over which temperature changes in the vertical. This thermocline depth D depends on the diffusive heat penetration, and a scaling can be obtained from an advective–diffusive balance [as in Munk's (1966) abyssal recipes] as $D = k/w$, where k is the vertical diffusivity and w the vertical velocity. Also using a continuity scaling $w = uD/L$ in (1) yields

$$w = \left(\frac{g\alpha}{2\Omega L^2}k^2\Delta T\right)^{1/3} \quad (2)$$

[similar scalings are discussed, e.g., by Welander (1986); F. Bryan (1987); K. Bryan (1991); and Weaver and Garrett (1993)]. Multiplication with a surface area (L^2) gives the desired estimate of thermohaline transport. Using typical values (ΔT = 20°C, k = 1 cm^2 s^{-1}, L = 5000 km) leads to a circulation of the order of 10 Sv (Sv $\equiv 10^6$ m^3 s^{-1}). A priori this overturning is *zonal,* since a meridional temperature gradient leads to zonal flow in the presence of rotation; Bryan (1987) has shown in the GFDL circulation model that, for restoring boundary conditions, zonal overturning indeed increases as $k^{2/3}$. *Meridional* overturning, which is the more interesting due to its importance for climate, is a secondary circulation set up by zonal pressure gradients resulting from the zonal flow, since the ocean is confined within continental boundaries. It also scales as $k^{2/3}$ in the GFDL model (Weaver and Garrett 1993; this revises the earlier finding of F. Bryan). This simple scaling has ignored the effects of salinity and wind forcing, and another caveat is that diffusivity k and temperature range ΔT are both not completely independent of the existing thermohaline circulation. In spite of these limitations, the scaling argument illustrates how the latitudinal temperature contrast at the surface, combined with vertical diffusion, will drive a deep circulation of the observed magnitude.

What is the local relation of sinking motions to convection? Convection patches are denser than the surrounding waters, or else convection would not occur. This leads to a high pressure region at depth. Due to the constraints of rotation, deep water cannot simply flow away from the dense patch as in Sandström's nonrotating tank experiments but circulates anticyclonically around it (Crepon et al. 1989). Nevertheless there will be a small ageostrophic component to the flow (due to instabilities and friction), which will lead to a flow divergence under the convection patch and convergence near the surface, connected by sinking. It is not clear, however, how strong this sinking is or whether this is the main mechanism causing the observed sinking. In the presence of preexisting flow, either caused by other convection nearby or by wind forcing, the situation is more complex (see, for example, the Ekman upwelling near the surface of the convection region along the northern model boundary in Fig. 3a, or Fig. 8c). In such cases no direct correspondence of convection and sinking exists; the preexisting flow can carry dense water out of the convection patch without divergence or sinking there. However, when convection is interrupted, the overturning circulation collapses within a few years in the models (see the model results described below). In this sense, convection "pushes" the thermohaline flow at least in coarse models, and when convection stops, the deep flow loses its driving force. In the long run, the thermodynamical "pull" of diffusion will start up convection and deep flow again, either in the same location or somewhere else.

b. *Mixed-boundary conditions and multiple steady states*

It is now well known that ocean models forced by mixed boundary conditions (i.e., fixed freshwater fluxes and a restoring condition on temperature) can have different equilibrium states, depending only on initial conditions. Marotzke and Willebrand (1991) have described four basic states of an idealized world ocean model: the "southern sinking" and "northern sinking" states and the "conveyor" and "inverse conveyor" states. However, in addition to these *qualitatively* different states, a large number of *quantitatively* differing equilibrium solutions can exist within each category for a given set of boundary conditions. For example, Hughes and Weaver (1994) have found conveyor belt states with different overturning rates in the Atlantic (e.g., 10, 22, 28, or 35 Sv) in their idealized World Ocean model.

Recently, Lenderink and Haarsma (1994) have demonstrated in a simple hemispheric ocean model how multiple equilibria can be caused by convection. Convection is to some extent a self-sustaining process: once convection has started at a certain location, it creates favorable conditions for further convection there. This is because stratification is removed and convection leads to increased surface heat loss by bringing up warmer water from deeper levels. This positive feedback allows some grid points of an ocean model to exist in two stable states, namely, with or without convection, depending only on initial conditions. By applying Welander's (1982) box model to individual grid points of their three-level geostrophic ocean model, Lenderink and Haarsma were able to show that a whole region of such "flip-flop" points lies in between the unconditionally convecting points at their northern model boundary and the unconditionally stable points in lower latitudes. Depending on which of the flip-flops are turned on or off, a large number of different model states are possible.

Could this mechanism apply also to more complex ocean models with many levels, and could it account

for such widely differing circulation states as found by Hughes and Weaver? In order to investigate the role of multiple convection states further, a series of model experiments were performed with the Geophysical Fluid Dynamics Laboratory (GFDL) modular ocean model, which are described and analyzed in this paper. In section 2 the model is described, in section 3 results with traditional mixed boundary conditions are shown; in section 4 the dynamical effects of convection are discussed; and in section 5 experiments with an implied coupling to a diffusive atmosphere are presented.

2. The ocean model

a. Model description

The model configuration used here is described in detail in Rahmstorf and Willebrand (1995; hereafter RW) (Fig. 1). It is a coarse-resolution (3.75° × 4°) implementation of the GFDL modular ocean model (MOM; Pacanowski et al. 1991, 1993), with 15 levels in the vertical. The domain consists of two basins of 60° width, which represent the Pacific and Atlantic Oceans and will be referred to as such. The basins are identical in geometry and of uniform depth (4500 m) and are linked in the south by a "circumpolar current" with a cyclic boundary condition joining 0° and 135° longitude. The transport of this current was prescribed to be 140 Sv.

The time step is 1.5 hours during times with rapid temporal changes, that is, the initial response of the model to a perturbation. Runs were then continued to equilibrium for several thousand years using split time stepping (Bryan 1984), extending the time step for the tracer equations to 1 day. Constant horizontal and vertical diffusivities ($K_H = 10^3$ m^2 s^{-1}, $K_v = 5 \cdot 10^{-5}$ m^2 s^{-1}) and viscosities ($A_H = 2.5 \times 10^5$ m^2 s^{-1}, $A_v = 10^{-4}$ m^2 s^{-1}) were applied. A fast convection scheme was used that completely removes all static instability at each time step (Rahmstorf 1993).

b. Forcing and spinup

The experiments to be described here use two alternative types of surface boundary condition, representing different couplings to the atmosphere. The first type is a traditional "mixed" boundary condition, prescribing fixed freshwater fluxes and computing heat fluxes from a restoring condition (this condition is labeled HR, for "Haney restoring"). The second type replaces the restoring condition on temperature with a more realistic thermal energy balance, representing a diffusive atmosphere (see RW):

$$Q = \gamma(T^* - T_o) - \mu\nabla^2(T^* - T_o). \qquad (3)$$

This condition has been labeled EB (for energy balance). In Eq. (3) Q is the heat flux at the ocean surface, T_o the ocean surface temperature, γ a radiative relaxation constant (3 W m^{-2} K^{-1}), and μ a constant related

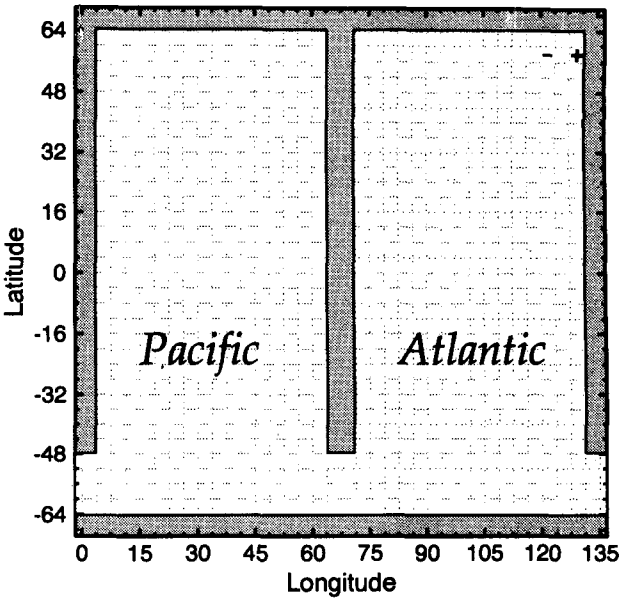

FIG. 1. The model domain. Two identical basins represent Pacific and Atlantic. The basins differ only in the circulation pattern: deep water is formed in the northern Atlantic but not in the northern Pacific basin. The "+" and "−" signs mark grid cells where a freshwater perturbation is added in two experiments.

to atmospheric heat diffusion (8×10^{12} W K^{-1}). The term T^* defines a climate without oceanic heat transport, around which Eq. (3) is linearized; T^* was prescribed as a cosine function of latitude, varying from 33°C at the equator to −4°C at the northern and southern model boundaries at ±64° latitude. In contrast to classical restoring, where the atmospheric temperature is assumed fixed and the heat flux from the ocean disappears into an "infinite sink" atmosphere, Eq. (3) represents a closed heat budget. Heat leaving the ocean can only be lost to space through longwave radiation (first term), or it can be redistributed laterally within the atmosphere by turbulent diffusion (second term). Atmospheric temperature is a diagnostic variable in this model, more closely tied to T_o than to T^*; from Eq. (3) it has already been eliminated by inserting the atmospheric heat budget equation.

An important difference between the two types of thermal forcing is in the sensitivity ($\partial Q/\partial T_o$) of the surface heat flux Q. Traditional restoring assumes a fixed atmospheric temperature to which the sea surface temperature T_o is tightly coupled ($\partial Q/\partial T_o = 80$ W m^{-2} K^{-1} in our case). The energy balance condition allows the air temperature to respond to changes in oceanic heat release, giving a coupling that depends on the spatial scale of SST anomalies. For large-scale phenomena, this coupling is much weaker than in the HR condition, and consequently SST is more variable. RW found a sensitivity of about 10 W m^{-2} K^{-1} resulting from Eq. (3) during transitions of the thermohaline circulation.

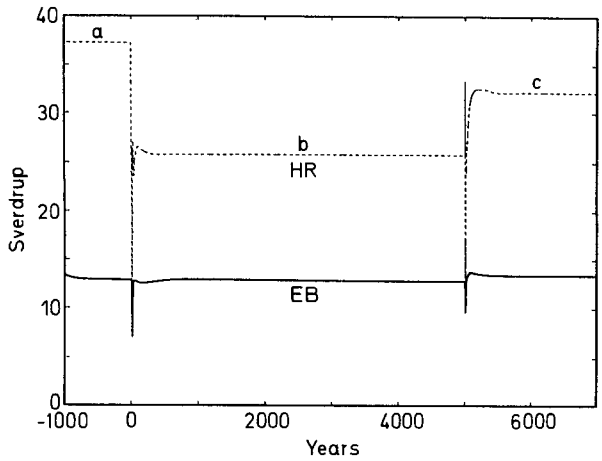

FIG. 2. Time series of the maximum of the deep overturning cell in the Atlantic. At years 0 and 5000 a freshwater perturbation is started that lasted for 4 years. The curve labeled EB shows the response with the surface heat balance of Rahmstorf and Willebrand (1995), while the curve labeled HR uses traditional Haney restoring.

The prescribed freshwater flux was derived in the same manner for both types of experiment. It was diagnosed from a spinup experiment where salinity was restored to a prescribed field (a simple cosine function of latitude, varying from 36 psu at the equator to 33 psu at the northern model boundary). This diagnosed flux was zonally averaged and then held fixed in all subsequent experiments.

The wind forcing consisted of a simple latitude-dependent zonal wind stress as pictured in Marotzke and Willebrand (1991).

A conveyor belt circulation was "kick started" by temporarily removing some freshwater from one basin (the "North Atlantic") while adding it to the other. Once the conveyor belt is running, it is self-sustaining due to salt advection from lower latitudes toward the North Atlantic sinking region, the well-known positive feedback originally described by Stommel (1961). After the flux anomaly used for the kick start is removed, the model is integrated for several thousand years until a steady equilibrium is reached. This spinup procedure can by now be considered standard and is therefore only summarized briefly here; for a more detailed discussion see RW.

3. Experiments with Haney restoring

The initial steady solution obtained by the spinup procedure described above (for the HR case, the traditional mixed boundary condition) is a conveyor belt circulation with a very strong meridional overturning of 37 Sv in the North Atlantic and a reverse overturning cell in the Pacific. (It is pictured in RW, their Fig. 16.)

This equilibrium state was perturbed by a temporary additional freshwater flux of 1.7 m yr^{-1} into the North Atlantic north of 56°N (equivalent to an inflow of 0.16 Sv), lasting for 4 years. It was then integrated further with the original freshwater forcing in order to establish the long-term response to the temporary perturbation.

The time series of the maximum overturning rate in the North Atlantic is shown in Fig. 2. The perturbation (during years 0–3) leads to a "polar halocline catastrophe" and collapse of the thermohaline circulation. The freshwater flux used in these experiments is not conducive to a "southern sinking" circulation state, and the conveyor recovers rapidly after the initial collapse. However, the new equilibrium reached after the perturbation has an overturning rate of only 26 Sv, compared to 37 Sv in the initial state. This conveyor equilibrium is shown in Fig. 3. The same perturbation was then applied again during model years 5000–5003. Again, the conveyor collapses and then recovers, this time to an overturning rate of 32 Sv. We thus have three different conveyor equilibria under the same surface conditions, with transitions between the states triggered by a brief freshwater release into the northern North Atlantic.

Figure 4 shows convection depth and convective heat loss in the North Atlantic for the three equilibrium states, as labeled in Fig. 2 (referred to as HR-a, HR-b, and HR-c). Clearly, very different convection patterns are associated with these three states. But are these patterns the *cause* or a mere side effect of the different strength of the conveyor circulation?

To test this, I performed a "surgical" freshwater perturbation on the HR-b conveyor state. This pertur-

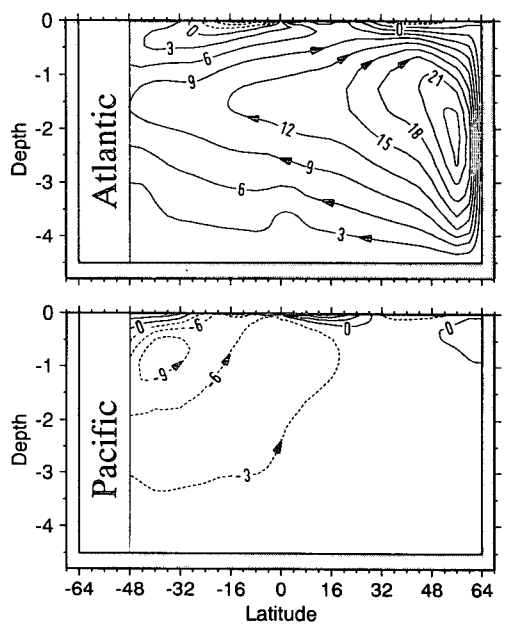

FIG. 3. Meridional overturning in the two model basins for the HR equilibrium labeled b in Fig. 2 (HR-b), with 26 Sv overturning. (a) Atlantic basin; (b) Pacific basin.

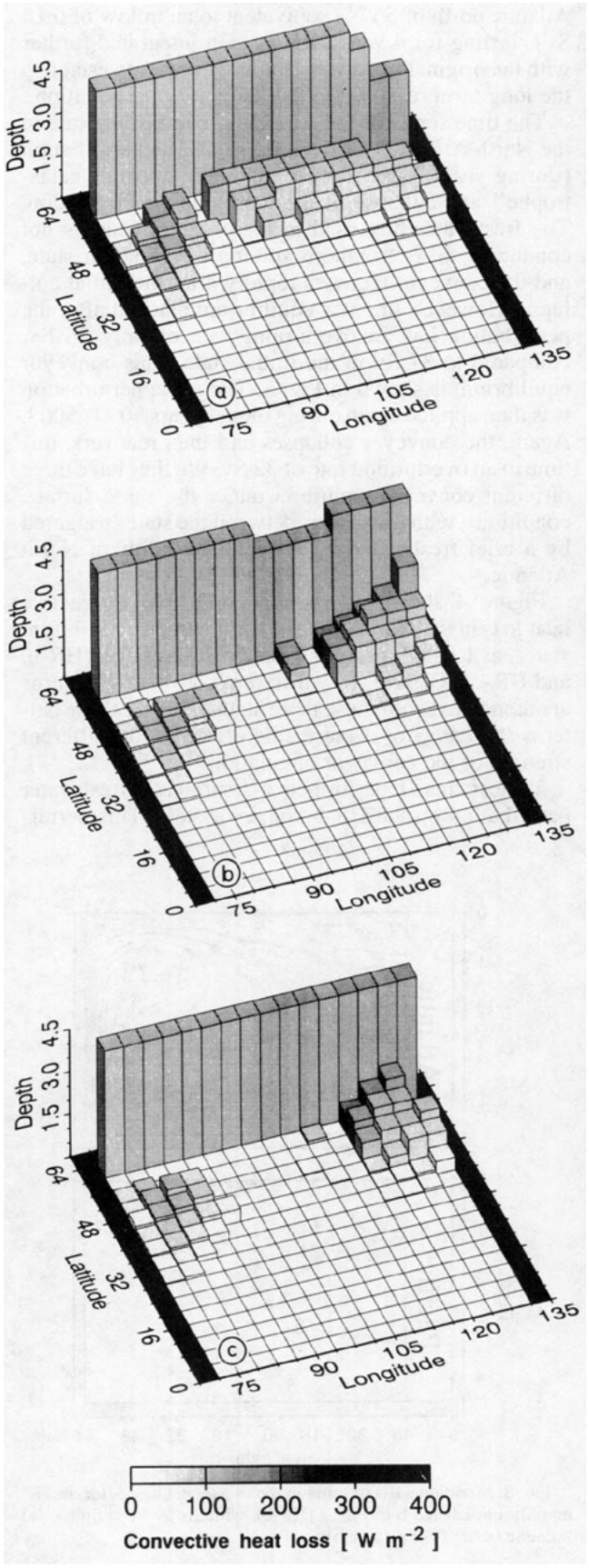

bation consisted of an additional freshwater flux of 2 m yr^{-1} added for 10 years to one grid point only (equivalent to 0.006 Sv) at the location marked "+" in Fig. 1. Figure 4b shows that this is a point with convection down to level 11 or 2100 m. The opposite perturbation (−2 m yr^{-1}) was added to a nearby point (marked "−"), so that the total freshwater input was zero. The resulting time series of overturning is shown in Fig. 5. Convection at point "+" is interrupted by the freshwater input; this sets off a chain reaction leading to a completely different convection pattern. The circulation responds dramatically, increasing to over 32 Sv before settling down at 30 Sv after the end of the perturbation. The experiment was repeated with an otherwise identical perturbation of smaller amplitude, 1.7 m yr^{-1}. This is just below the threshold where convection at point "+" is flipped to the *off* state, and the circulation is hardly affected.

These results demonstrate that changes in the convection pattern of the model can indeed cause large changes in the deep water formation rate. In Fig. 2 the convection pattern is completely erased during both perturbations by a large-scale freshwater cap, and a new pattern with a new circulation arises after the fresh water is dispersed. The surgical perturbation (Fig. 5) triggered a similar transition between two convection patterns by turning off one convection point and stimulating another.

4. Dynamics of the convection-driven flow field

How can the distribution of convection points control the model's overturning? In order to investigate this question, we take a close look at the differences between two of the conveyor equilibria. The two equilibria HR-b and HR-c were chosen. These have Atlantic overturning cells of 26 Sv and 32 Sv, respectively, under the same boundary conditions, and this difference is caused by only a small change in convection pattern (Fig. 4). These runs therefore provide a unique laboratory for investigating the dynamics of deep water formation driven by convection, as it occurs in a coarse-resolution model.

Figure 6 shows the difference in meridional overturning in the Atlantic between the two runs. It is immediately obvious that the difference is confined largely to the two or three northernmost grid rows. This does not mean that the mechanism is unimportant for the large-scale flow, however. Experiments with dif-

FIG. 4. Convection patterns in the North Atlantic for the three equilibria of the HR run shown in Fig. 2. Convection depth (in km) at each grid cell is plotted as a vertical bar. (a) HR-a state, (b) HR-b state, (c) HR-c state. Shading shows the heat loss associated with convection at each grid point (defined as convective heat flux through model level 1).

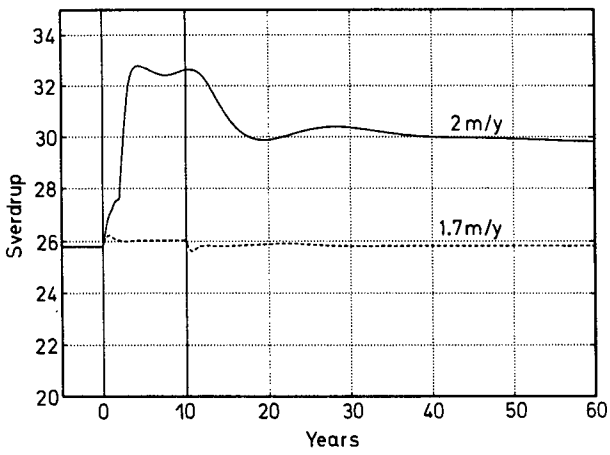

FIG. 5. Time series of the maximum of the deep overturning cell in the Atlantic for the experiments with a "surgical" freshwater perturbation at the points marked in Fig. 1.

ferent thermal forcing, described below, and some preliminary studies with a realistic topography global ocean model (to be published elsewhere) indicate that rearrangements of the convection patterns can have far-reaching consequences on a basin-wide scale. Only in the simple case discussed here is the effect so localized, and this simplifies the analysis.

Figure 7 shows close-ups of the North Atlantic model basin at four different depth levels. The density difference between the two runs is indicated by shading. The dark shades highlight the points where there is convection in run HR-b but not in run HR-c. These are also points of extra surface heat loss of up to 250 W m^{-2} (not shown). This heat loss is largely balanced by reduced heat loss along the whole northern boundary of the basin, consistent with the flow pattern described below. Also shown in Fig. 7 is the difference in velocity between the two equilibria, driven by the density differences. Horizontal velocities in this model (which uses a B grid) are computed at the corners of the grid cells and are indicated by arrows. Vertical velocities are indicated by circles (upward) or crosses (downward), and they apply at the bottom center of each grid cell.

The ocean model is hydrostatic, so that the vertical velocities are not computed prognostically but rather from the divergence of the horizontal flow. (Convection is handled in the model as mixing of unstable levels and does not directly cause any vertical flow.) The equilibrium horizontal flow in this coarse flat-bottomed model is essentially determined by a balance between pressure gradient, Coriolis force, and friction; the nonlinear terms in the momentum equation are negligible since the Rossby number is small even on grid-length scale. The geostrophic flow component is practically nondivergent [at least for flows of a small scale compared to the equator–pole distance; see Pedlosky (1987, 54f)], so that it will not generate vertical velocities. This holds also in the finite-difference formulation of the GFDL model. In case of a density anomaly adjacent to a land boundary, however, the "no slip" and "no normal flow" conditions at the boundary force zero velocities there and prevent closed geostrophic flow; upwelling to the north and downwelling to the south of the density anomaly result (Fig. 8). In the interior only the ageostrophic component of the flow, caused by friction, instigates sinking or rising motions.

Figure 7 shows that two convection points at the eastern wall cause strong downwelling, which is the main cause of the change in overturning seen in Fig. 6. Four adjacent convection points in the interior, in contrast, cause cyclonic surface flow but only little downwelling. Looking at deeper levels, we see that the density anomaly at the eastern wall reaches a greater depth than the anomaly in the interior. The depth-integrated density anomaly is therefore much larger, although the surface manifestation is similar in size. This raises the question of whether the downwelling at the eastern boundary is stronger because of the interaction of the geostrophic flow with the boundary (discussed above) or simply because the density anomaly is deeper there. Comparison of Fig. 7 with the purely geostrophic effect shown in Fig. 8 suggests that the ageostrophic, frictional component dominates, which could also generate sinking in the interior. This is not surprising, as the viscosity in these coarse models is deliberately chosen large enough to spread boundary flows over several grid points.

Thus far we have only discussed the flow *directly* forced by the density anomaly in its immediate vicinity, which can be analyzed in terms of geostrophy and friction. The remainder of the flow, associated with advected changes in the density field, is best understood in terms of vorticity dynamics. The downwelling caused by the density anomaly provides a deep source of dense water that spreads most easily along lines of constant potential vorticity, that is, along latitude cir-

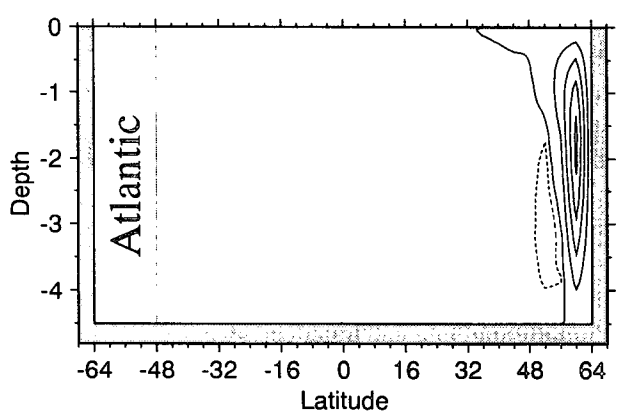

FIG. 6. Difference plot of the meridional mass transport (Sv) in the Atlantic basin, equilibrium HR-c minus HR-b. Contour interval 3 Sv for the positive contours and 1 Sv for the negative contour.

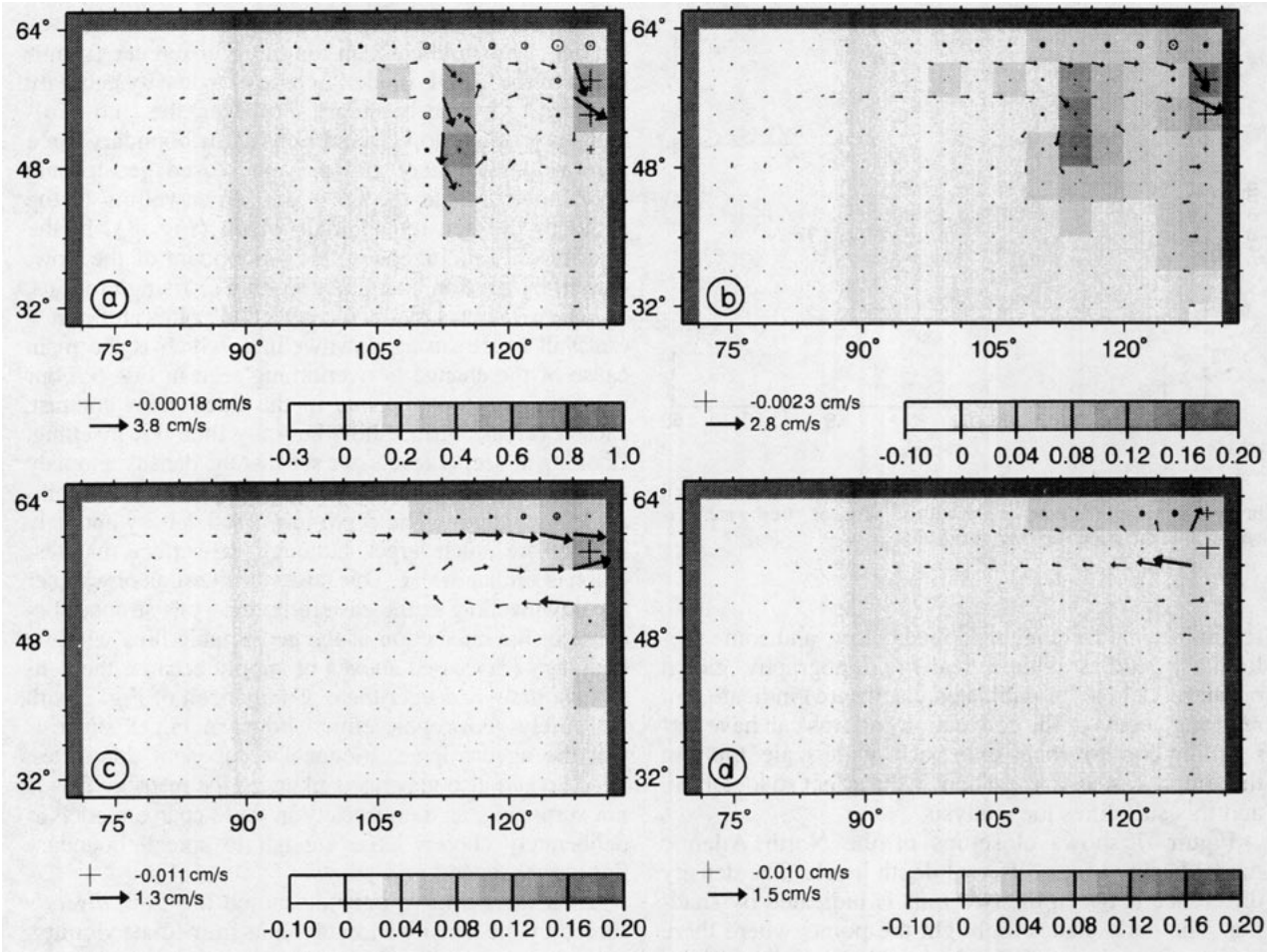

FIG. 7. Difference plot of density and flow pattern in the northern Atlantic, equilibrium HR-b minus HR-c. Arrows show relative horizontal flow, circles upwelling, and crosses downwelling, while shading indicates density differences (kg m^{-3}). (a) Model level 1, 12.5 m; (b) level 5, 258 m; (c) level 10, 1455 m; and (d) level 13, 2929 m. (These depths are for the center of each model level, where density and horizontal velocity is calculated. Vertical velocities apply at the bottom of each level.)

cles (Fig. 7d). In the shallower levels (Figs. 7a–c) we see the return flow of this water, which is required because the thermohaline flow has to be entirely baroclinic in a coarse flat-bottomed model. Friction slows down this deep plume farther from its source, leading to convergence and upwelling and giving the plume a northward component ($\beta v = f\partial w/\partial z$). This gives rise to the upwelling along the northern model boundary, which closes the meridional cell seen in Fig. 6. This kind of buoyancy-driven flow pattern is described by "β plume" theory (see, e.g., Rhines 1993).

It is clear that the secondary large-scale flow set up by convection favors upwelling or downwelling at land boundaries, causing convergence where it "runs into the wall." This can make the vertical overturning of the model dependent on the zonal distribution of convection, so that in our three-dimensional model there is no unique relationship between meridional flow and zonally averaged density distribution. Such a relationship is usually postulated in two-dimensional circulation models (e.g., Marotzke et al. 1988; Wright and Stocker 1991).

5. Experiments with energy balance atmosphere

It is now widely recognized that the traditional restoring boundary condition for temperature, which was used in the runs discussed so far, artificially constrains the surface temperature of the model and precludes important feedback effects. It is therefore not well suited for the study of multiple equilibria and makes the ocean model oversensitive to the kind of perturbations used for the experiment shown in Fig. 2. In RW the authors proposed an energy balance boundary condition that overcomes some of this shortcoming by taking into account the atmospheric response to changes in SST in a simple way.

The series of perturbation experiments were repeated with this more realistic thermal boundary condition

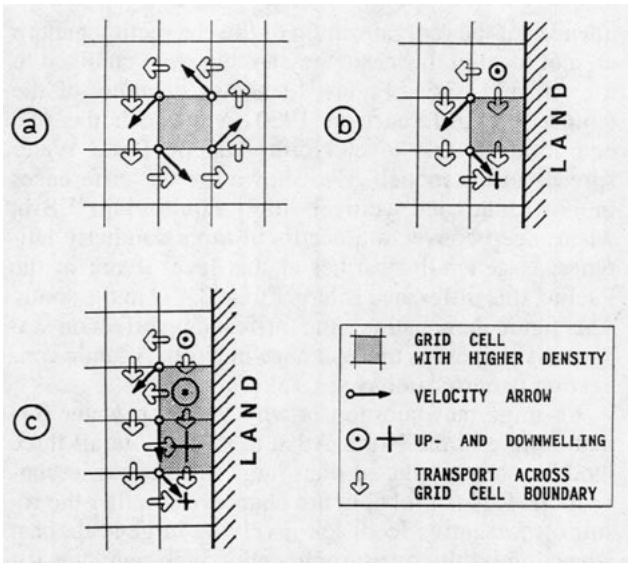

FIG. 8. Geostrophic component of the surface velocity and associated vertical flows as calculated in the model grid for three simple cases: (a) one dense grid column surrounded by fluid of uniform density, (b) one such column adjacent to a land boundary, and (c) two adjacent dense columns. The dense columns correspond to a situation caused by steady convection, see Fig. 7. Geostrophic velocity components are computed by the model at corner points using the four adjacent grid boxes; their average north–south density gradient yields the u component, the average east–west gradient the v component. Transports across box boundaries are then computed from the average velocity component across the boundary at the two adjacent velocity points. Finally, vertical velocities are computed from these lateral transports in and out of the box by applying the continuity equation. The figure is meant to clarify these steps. Note that in principle there can be upwelling in a dense grid column (c).

(using the same freshwater flux as before), and the results are shown in Fig. 2 (curve labeled EB). Because it is harder to interrupt convection with this boundary condition (see RW for a quantitative estimate of this effect), the freshwater perturbation had to be twice as strong as in the HR experiment to trigger the desired state transitions. As in the run labeled HR, the circulation collapses temporarily after each freshwater input and reestablishes itself in a different equilibrium state with a very different convection pattern in the North Atlantic (shown in Fig. 9). However, the three different equilibrium states here have very similar overturning rates (between 12.8 and 13.4 Sv).

Meridional mass transport in the Atlantic basin is shown in Fig. 10 for these three states. It is important to keep in mind that these are three realizations under the same boundary conditions. A new feature, which does not arise in the HR runs, is the Antarctic Bottom Water cell coming northward into the Atlantic, discussed in RW. In Figs. 10b and 10c, this cell penetrates right up to the northern model boundary, and no convection reaches the bottom there. Figure 10b differs from the two other states in that there is no zonal-mean outflow of North Atlantic deep water into the circumpolar region.

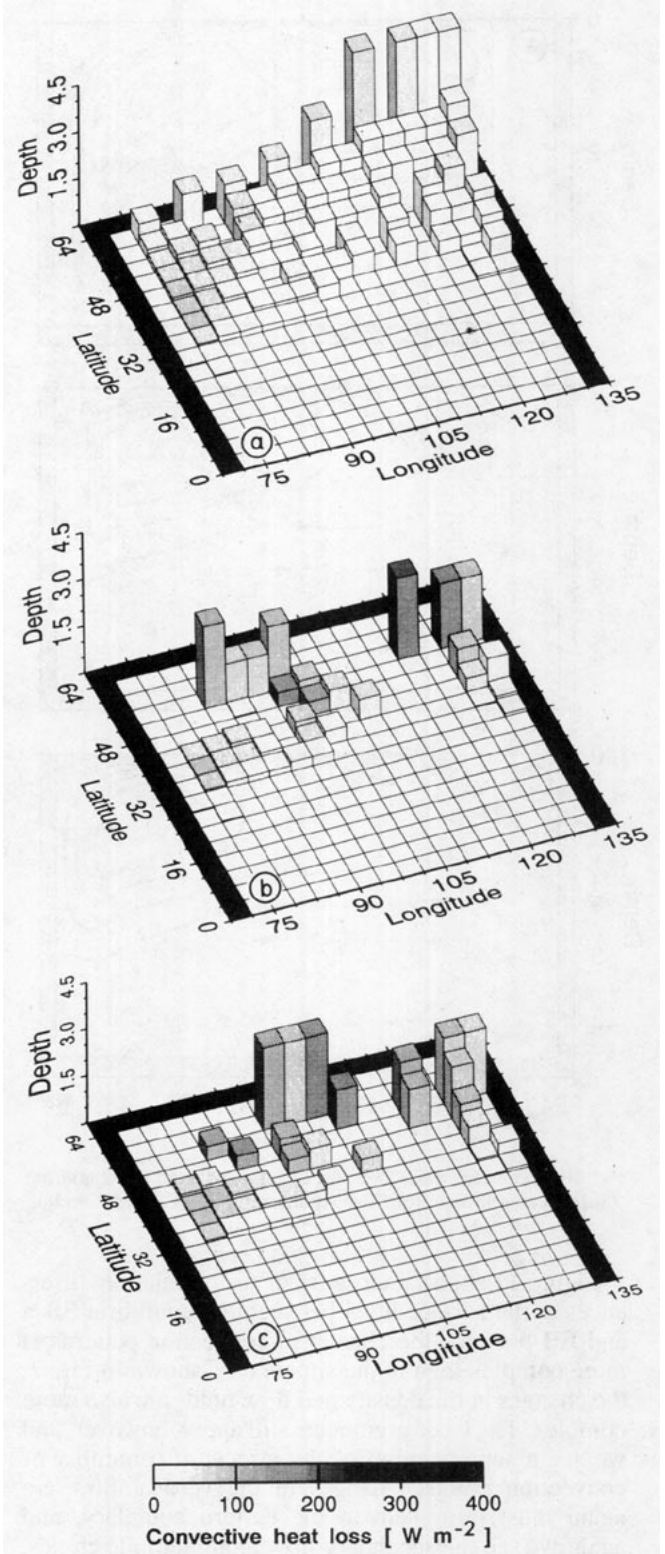

FIG. 9. Convection patterns in the North Atlantic for the three equilibria of the EB run shown in Fig. 2. Convection depth (in km) at each grid cell is plotted as a vertical bar. (a) EB-a equilibrium, (b) EB-b equilibrium, (c) EB-c equilibrium. Shading shows the heat loss associated with convection at each grid point (defined as convective heat flux through model level 1).

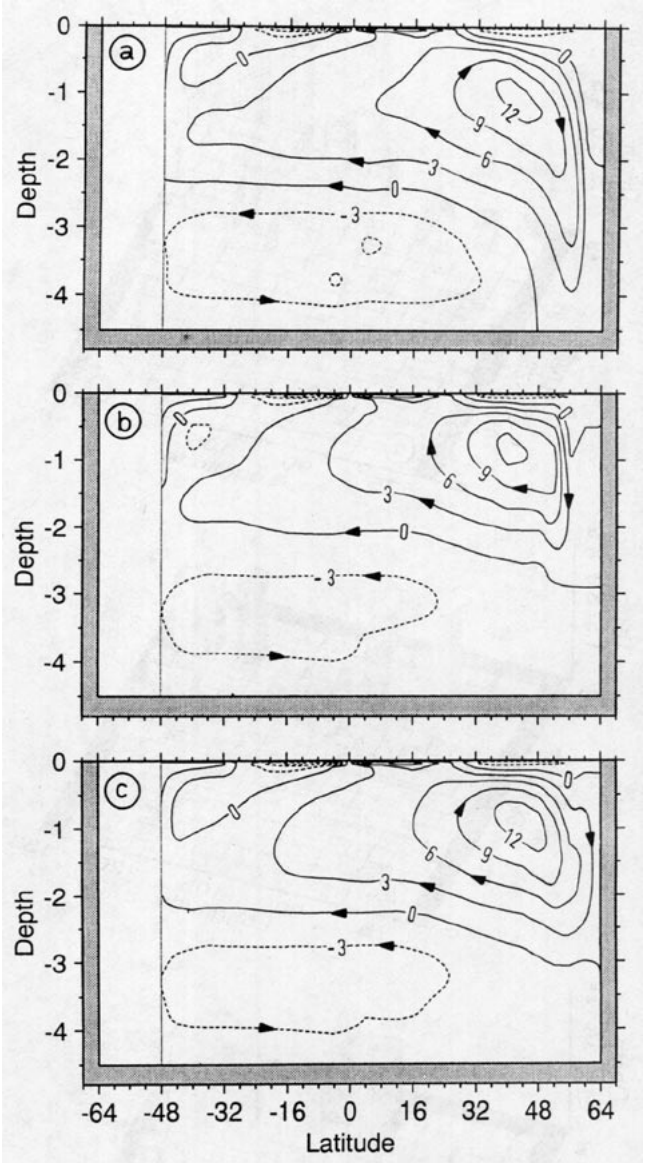

FIG. 10. Meridional mass transport (Sv) for the three EB equilibria: (a) EB-a equilibrium, (b) EB-b equilibrium, (c) EB-c equilibrium.

Figure 11 shows a close-up of the circulation differences at the surface level between the equilibria EB-a and EB-b. Since the change in convection patterns is more complex than in the simple case shown in Fig. 7, the changes in the density and flow fields are also more complex. The basic arguments still apply, however, and we see a superposition of the effects of a number of convection points. Changes in the vertical flow are again most prominent at the eastern boundary, and again we see the secondary flow along latitude circles, feeding the sinking regions. A new feature is that this density difference field induces a change in the western boundary current.

This points at a major difference from the simple case discussed in the previous chapter: the consequences of the reorganization of the convection pattern are not local in this case; they are not even confined to the Atlantic basin. Figure 12 shows contours of the temperature difference at 1900 m between the two equilibria; at this level North Atlantic Deep Water spreads in the model. Also shown are the differences in horizontal and vertical flow. Equilibrium EB-b, where deep convection occurs in more southerly latitudes, is generally warmer at this level. Even in the Pacific, this difference is larger than 0.4°C in the south. This figure demonstrates the far-reaching effect on water mass properties that a change in North Atlantic convection pattern can have.

An important question is why the deep water formation rate in the North Atlantic is 13 Sv in all three model states in spite of their large differences in convection. This is probably not chance, but rather the result of a negative feedback involving large-scale heat advection by the overturning cell, which regulates the deep water formation rate: if it increases, more warm water is advected to the deep water formation region, which increases the temperature and thus decreases the density there, inhibiting convection (see RW). This feedback is largely suppressed in the HR run due to the strong coupling to a fixed atmospheric temperature, accounting to some extent for the extreme sensitivity of models with classical mixed boundary conditions.

We can estimate whether this proposed feedback is strong enough to be responsible for stabilizing the over-

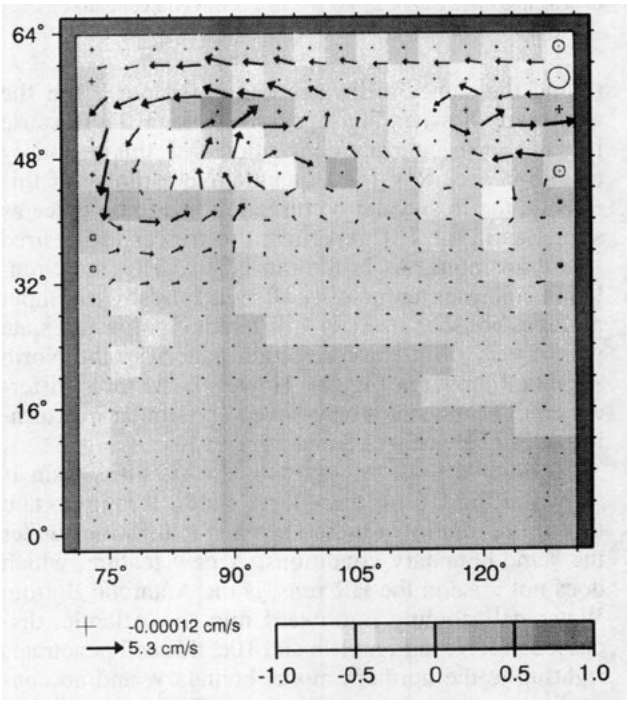

FIG. 11. Difference plot of density and flow pattern in the northern Atlantic at level 1, equilibrium EB-b minus EB-a. Arrows show relative horizontal flow, circles upwelling, and crosses downwelling, while shading indicates density differences (kg m^{-3}).

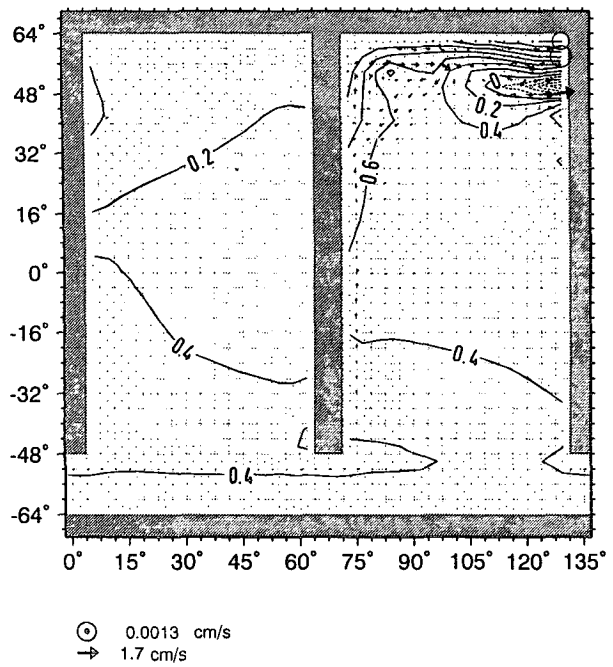

FIG. 12. Difference plot of temperature and flow pattern at level 11 (1882 m), equilibrium EB-b minus EB-a. Arrows show relative horizontal flow, circles upwelling and crosses downwelling, while contours show temperature differences (degrees).

turning rate. One way of doing this is to compare the conditions in high latitudes with and without overturning. In our idealized model we can use the Pacific basin as a "control" basin without overturning, since its geometry and forcing is identical to the Atlantic basin; all differences are caused by the conveyor circulation. Comparing average conditions north of 48°N (where the overturning maximum is situated), we find that the Atlantic is 2.0 psu saltier than the Pacific in equilibrium Eb-a, and also 5.3°C warmer. The enhanced salinity is of course part of the positive feedback that drives the conveyor, while the increased temperature tends to slow it down. How strong is the braking effect of this temperature rise? The average surface density in the Pacific north of 48°N is 1025.6 kg m^{-3}, in the Atlantic it is 1026.5. To separate out the temperature effect, we estimate the density that the North Atlantic would have without the 5.3°C temperature rise. This is 1027.2 kg m^{-3}, which means that the surface density increase resulting from the 13 Sv overturning would be approximately 1.6 kg m^{-3} due to salinity alone but is reduced to 0.9 kg m^{-3} by the temperature feedback.

A similar analysis can be done by comparing the conditions for the three different EB equilibria. The northern Atlantic salinity drops from 34.2 psu in EB-a to 33.4 in EB-b, and the temperature drops from 8.4° to 5.8°C. The salinity change alone would cause a density decrease by 0.7 kg m^{-3}, but temperature compensates more than one-half of this, leading to an actual density decrease of only 0.3 kg m^{-3}. Of course, changes in average surface density are only a rough indication of the effect on flow, which depends on where the convection occurs, as we have seen above. These estimates demonstrate, however, that the advective temperature changes are of the right magnitude (compared to the salinity changes) to produce a powerful feedback.

An attempt was made to "kick" the model into a stronger overturning mode by adding a -1 m yr^{-1} freshwater flux anomaly north of 44°N in the Atlantic and a corresponding anomaly of opposite sign in the Pacific (to conserve total salinity) during a time interval of 1000 years. The enhanced salinity of the North Atlantic indeed boosted overturning to 22 Sv at first, settling down to 18 Sv after about 200 years. However, after the perturbation was removed, overturning quickly dropped back and settled at the original 13 Sv. This experiment again supports the idea that for a given freshwater flux and EB thermal coupling, there is a powerful negative feedback regulating the overturning rate.

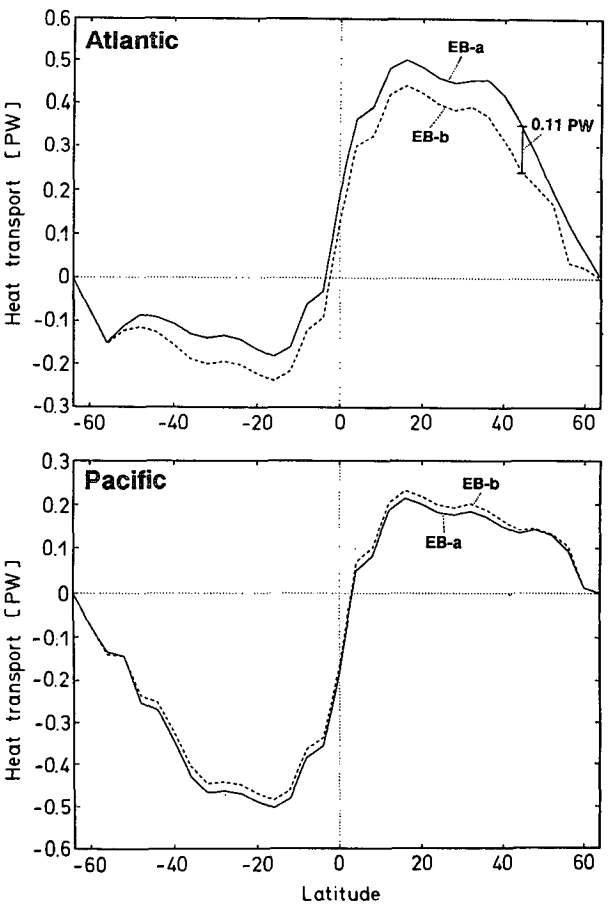

FIG. 13. Meridional heat transport in the Atlantic (top) and Pacific (bottom) for equilibria EB-a and EB-b. Northward heat transport in the Atlantic is reduced by up to 0.11 PW (PW = 10^{15} W) in EB-b due to the southward shift in convection.

Although the discussed feedback strongly stabilizes the deep-water formation rate, it does not prevent climatic changes resulting from transitions in the circulation. The transition from EB-a to EB-b demonstrates this clearly. The freshwater release only briefly interrupts convection, and deep-water formation recovers quickly to its former value. But the northern Atlantic climate has cooled dramatically (see Rahmstorf 1994, his Fig 3). As a result of the shift in convection sites, the average surface temperature north of 44°N has dropped by 2.3°C, and the abyssal Atlantic has been cut off from ventilation by deep convection. Instead, Antarctic Bottom Water has pushed north to fill the entire abyssal Atlantic. This situation resembles the "glacial mode" of the conveyor belt as reconstructed by Sarnthein et al. (1994) from sediment core data. Rahmstorf (1994) discusses the climatic implications of these circulation changes and their possible links to glacial climate transitions in more detail.

The mechanism through which the shift in convection sites affects basinwide surface temperatures is the warming of the deep Atlantic outflow shown in Fig. 12 and discussed above. This is associated with reduced heat transport of the conveyor since this heat transport arises from the conveyor's mass transport multiplied by the temperature difference between warm inflow and cold outflow. The change in oceanic heat transport is shown in Fig. 13. While the heat transport in the Pacific basin differs little between the two equilibria, the Atlantic heat transport is reduced markedly in EB-b. The difference peaks at 0.11 PW at 44°N. By dividing this by the ocean surface area north of this latitude, we obtain an average change in surface heat flux (which must balance the transport change) of 13 W m^{-2}. If only radiative heat loss was allowed [first term of Eq. (3)], this would imply an SST change of 4.2°C, rather than the 2.3°C found with the full Eq. (1). This demonstrates how the atmosphere takes over part of the reduced heat transport of the ocean in our boundary condition Eq. (3).

6. Discussion

The author has shown that an OGCM under mixed boundary conditions can have many different equilibrium states caused by the fact that for a given surface forcing many different convection patterns can be stable [a mechanism first described by Lenderink and Haarsma (1994)]. Which convection pattern is established depends on the initial conditions. Initial conditions were changed by adding a brief surge of fresh water to the convection region in the Atlantic, which temporarily interrupts convection. After about 10 years convection starts up again, but in a different pattern. A more controlled method to change convection patterns, by switching off a single convection point, was also applied in one experiment.

Using Haney restoring on temperature, the model circulation is extremely sensitive to changes in North Atlantic convection pattern and responds with widely differing deep-water formation rates. With a more realistic thermal energy balance, in contrast, the overturning rate is hardly affected by the distribution of convection points; it is regulated by a negative feedback, involving the advection of heat toward the sinking region. In spite of the stable zonal-mean *mass* transport, the climate in the North Atlantic region can change dramatically between different model equilibria because the conveyor's *heat* transport depends on the temperature of the deep branch, which in turn depends on where deep water is formed. Water mass properties are affected even in the Pacific basin of the model.

The way in which convection affects the model's density field and circulation was analyzed in some detail. Convection creates a dense water column with cyclonic flow near the surface and anticyclonic flow at depth. It tends to cause convergence in the upper region and divergence at depth, due to frictional effects and interactions with boundaries. A β-plume circulation reaches out westward from the convection sites and feeds the inflow and outflow. Interactions of this secondary flow with land boundaries reinforce the tendency for sinking or upwelling to occur there. Not only the meridional, but also the zonal, distribution of convection points can affect the meridional flow.

In a coarse hydrostatic model such as the one used here, convection works by vertically homogenizing a large grid cell (up to 400-km side length), and consequently many modelers have strong reservations about how realistic this representation can be. In reality, convection occurs in small scale plumes ($\sim$1 km, see, e.g., Jones and Marshall 1993). Send and Marshall (1995) conclude, however, that the gross dynamical and water mass modification effect of these plumes is merely achieved by vertical mixing and that they do not directly cause significant net vertical flow. They estimate that the vertical mixing time is of the order of one day. This is the length of a tracer time step in our model and a very short time compared to the timescales of the large-scale circulation, so that the instantaneous mixing of unstable water columns seems justified in this context.

Both theoretical studies (Crepon et al. 1989) and recent models (Legg and Marshall 1993) show that the circulation set up once a convection patch is vertically mixed consists of a cyclonic gyre, or rim current, at the surface and anticyclonic flow at depth. These are roughly represented in the coarse model even for a single convective grid cell. What we cannot represent are the instability processes that laterally draw water into the convection patch; these have to be parameterized by an eddy viscosity in a coarse model. The basin-scale outflow of deep water from the convection regions can then again be resolved by the coarse model. The main criticisms of the handling of convection in coarse ocean models are then perhaps the way in which convergence of surface water into the convection patch is generated by viscosity and interactions with land

boundaries and that a convection patch in a $4 \times 4°$ model is necessarily somewhat large. The actual vertical mixing scheme, however, may be better than its reputation and, in fact, quite adequate for the purpose.

The strong horizontal diffusion in this type of model may lead to excessive convection in areas of strong horizontal gradients, where diffusive tracer transports can destabilize the water column. If a more realistic isopycnal mixing scheme is used (Danabasoglu et al. 1994), much of the deep water ventilation occurs slantwise along isopycnals rather than by vertical convection. Further study will have to determine how their parameterization will affect the dependence of model equilibria on convection sites discussed in this paper.

Another caveat is the smooth and steady forcing used in the model experiments reported here. To what extent a model may "lock in" to particular convection sites in the presence of a seasonal cycle or stochastic noise has not been investigated thus far. Since the water column can "remember" the effect of past convection events for some years, a seasonal cycle with winter convection may not affect the preference of convection to reoccur at the same spots. Stochastic noise with decadal timescales, on the other hand, could shift the model between different convection states more or less frequently, depending on its amplitude and spatial distribution. This may be the mechanism for the climate transitions described by Weaver and Hughes (1994). The smoothness of the zonal-mean forcing and the lack of realistic coastlines and topography in our model means that there is little to constrain convection sites. Realistic surface forcing would have much more structure related to geographical features and atmospheric circulation patterns, allowing only a limited number of possible convection locations. The general mechanism remains valid, however, and multiple convection patterns are also found in a realistic topography global ocean model (Rahmstorf 1995).

Multiple convection patterns are an important aspect of ocean model behavior under realistic boundary conditions. They can affect the deep water properties, the heat transport of the deep circulation, and thus the climate of the model. I suggest that they can probably arise in the coupled ocean–atmosphere models presently used for climate predictions. Changes in oceanic convection patterns, triggered by the act of coupling or by intrinsic atmospheric variability, could play a significant but as yet overlooked role in these models.

Acknowledgments. I am grateful to Jürgen Willebrand for his continual support of my work and to Peter Rhines and Uwe Send for stimulating discussions. This work was funded by the Deutsche Forschungsgemeinschaft (SFB 133). Computations were performed at the German Climate Computer Centre in Hamburg.

REFERENCES

Bryan, F., 1987: Parameter sensitivity of primitive equation ocean general circulation models. *J. Phys. Oceanogr.*, **17**, 970–985.

Bryan, K., 1991: Poleward heat transport in the ocean. *Tellus*, **43**, 104–115.

Colin de Verdière, A., 1993: On the oceanic thermohaline circulation. *Modelling Oceanic Climate Interactions*, Springer, 151–183.

Crepon, M., M. Boukhtir, B. Barnier, and F. Aikman III, 1989: Horizontal ocean circulation forced by deep-water formation. Part I: An analytical study. *J. Phys. Oceanogr.*, **19**, 1781–1793.

Danabasoglu, G., J. C. McWilliams, and P. R. Gent, 1994: The role of mesoscale tracer transports in the global ocean circulation. *Science*, **264**, 1123–1126.

Dickson, R. R., J. Meincke, S. A. Malmberg, and A. J. Lee, 1988: The "Great Salinity Anomaly" in the northern North Atlantic, 1968–82. *Progress in Oceanogr.*, Vol. 20, Pergamon, 103–151.

Hughes, T. M. C., and A. J. Weaver, 1994: Multiple equilibria of an asymmetric two-basin ocean model. *J. Phys. Oceanogr.*, **24**, 619–637.

Jones, H., and J. Marshall, 1993: Convection with rotation in a neutral ocean: A study of open-ocean deep convection. *J. Phys. Oceanogr.*, **23**, 1009–1039.

Legg, S., and J. Marshall, 1993: A heton model of the spreading phase of open-ocean deep convection. *J. Phys. Oceanogr.*, **23**, 1040–1056.

Lenderink, G., and R. J. Haarsma, 1994: Variability and multiple equilibria of the thermohaline circulation, associated with deep water formation. *J. Phys. Oceanogr.*, **24**, 1480–1493.

Marotzke, J., and J. Willebrand, 1991: Multiple equilibria of the global thermohaline circulation. *J. Phys. Oceanogr.*, **21**, 1372–1385.

——, P. Welander, and J. Willebrand, 1988: Instability and multiple steady states in a meridional-plane model of the thermohaline circulation. *Tellus*, **40A**, 162–172.

Munk, W. H., 1966: Abyssal recipes. *Deep-Sea Res.*, **13**, 707–736.

Pacanowski, R., K. Dixon, and A. Rosati, 1991,93: The GFDL modular ocean model users guide. Vol. 2, GFDL.

Pedlosky, J., 1979, 1987: *Geophysical Fluid Dynamics*. Springer, 710 pp.

Rahmstorf, S., 1993: A fast and complete convection scheme for ocean models. *Ocean Modelling*, **101**, 9–11.

——, 1994: Rapid climate transitions in a coupled ocean–atmosphere model. *Nature*, **372**, 82–85.

——, 1995: Climate drift in an OGCM coupled to a simple, perfectly matched atmosphere. *Climate Dyn.*, in press.

——, and J. Willebrand, 1995: The role of temperature feedback in stabilizing the thermohaline circulation. *J. Phys. Oceanogr.*, **25**, 787–805.

Rhines, P. B., 1993: Oceanic general circulation: Wave and advection dynamics. *Modelling Oceanic Climate Interactions*, Springer, 67–149.

Sandström, J. W., 1908: Dynamische Versuche mit Meerwasser. *Ann. Hydrogr. Marit. Meteor.*, **36**, 6–23.

Sarnthein, M., K. Winn, S. J. A. Jung, J. C. Duplessy, L. Labeyrie, H. Erlenkeuser, and G. Ganssen, 1994: Changes in east Atlantic deepwater circulation over the last 30,000 years: Eight time slice reconstructions. *Paleoceanogr.*, **9**, 209–267.

Send, U., and J. Marshall, 1995: Integral effects of deep convection. *J. Phys. Oceanogr.*, **25**, 855–872.

Stommel, H., 1961: Thermohaline convection with two stable regimes of flow. *Tellus*, **13**, 224–230.

Weaver, A. J., and J. R. Garrett, 1993: On the sensitivity of the thermohaline circulation in ocean general circulation models to the vertical eddy diffusivity. (Unpublished manuscript.)

——, and T. M. C. Hughes, 1994: Rapid interglacial climate fluctuations driven by North Atlantic ocean circulation. *Nature*, **367**, 447–450.

Welander, P., 1982: A simple heat-salt oscillator. *Dyn. Atmos. Oceans*, **6**, 233–242.

——, 1986: Thermohaline effects in the ocean circulation and related simple models. *Large-Scale Transport Processes in Oceans and Atmosphere*, Reidel, 163–200.

Winton, M., and E. S. Sarachik, 1993: Thermohaline oscillations induced by strong steady salinity forcing of ocean general circulation models. *J. Phys. Oceanogr.*, **23**, 1389–1410.

Wright, D. G., and T. F. Stocker, 1991: A zonally averaged model for the thermohaline circulation. Part I: Model development and flow dynamics. *J. Phys. Oceanogr.*, **21**, 1713–1724.